Chapter 3

Studies on photocatalytic degradation of MB with Lanthanum doped TiO_2 nanoparticles

Abstract:

In this study, bare and Lanthanum (La) doped TiO_2 photocatalysts $Ti_{1-x}La_xO_2$ (x= 0.00-0.025) were prepared by employing a solution-combustion procedure. In this citric acid was utilised as fuel and as a complexing agent. The prepared photocatalysts were characterized by FTIR, FE-SEM, XRD, DRS and XPS. The XRD confirms that prepared TiO_2 photocatalysts have only the anatase phase and also crystallite size was calculated which is 30.16 and 19.90 nm for bare and $Ti_{0.985}La_{0.015}O_2$ respectively. The DRS shows that with increasing the doping concentration of La in TiO_2, a continuous shifting in absorbance towards the visible light region was observed. The FTIR determine the O-H band, Ti-O-La and several other functional groups present in the synthesized bare and La doped TiO_2 photocatalysts. The XPS spectra confirm the existence of all expected elements (Ti, O, and La) in the synthesized photocatalysts. The FE-SEM confirms spherical shape of prepared photocatalysts and particle size of bare and $Ti_{0.985}La_{0.015}O_2$ were 32.28 and 22.24 nm respectively which agrees with XRD data. Photo-catalytic breakdown of Methylene blue (MB) dye in its aqueous solutions of different concentrations (10, 20, 30, 40 and 50 ppm) was found to be first order. The best activity was shown by $Ti_{0.985}La_{0.015}O_2$ and it was better than the commercial Aeroxide P-25 photocatalyst. The $Ti_{0.985}La_{0.015}O_2$ catalyst could be regenerated and reused up to five times with a minor loss in degradation efficiency of MB dye (30 ppm) about 7.85% at the end of fifth cycle however with fresh catalyst degradation was 88.71%.

3.1 Introduction

This work focuses on synthesising undoped and La-doped TiO_2 nanoparticles utilising cost-effective TiO_2 powder. La doping promotes the separation of electrons and holes and reduces rate of recombination of the charge carrier and hence La doping improves TiO_2 photo reactivity. The synthesis process involves a solution combustion method using citric acid as a fuel and subsequent calcination to enhance the crystallinity. This method creates fine TiO_2 particles by limiting their growth, which is easy and cheap. The degradation of the MB dye in the UV Photochemical reactor served as the basis for investigating the photocatalytic performance of the photocatalysts. The Table 3.1 mentions a brief of studies related to La doped TiO_2's use in degradation of various pollutants.

Table 3.1 Previous Literature related to La doped TiO_2

S.N.	Dopant Level	Pollutant	Intial conc.	Results	Ref.
1.	1.5% mole	Methyl Orange	20 ppm	77.48% degradation in 8h under visible light	[1]
2.	1% wt.	Phoxim	20 ppm	Almost 100% degradation in 4h under UV light	[2]
3.	3% wt.	NO	50 ppm	29% degradation in 30 min under visible light	[3]
4.	5% wt.	Diclofenac	50 ppm	Degradation under UV and visible light.	[4]
5.	5% mole	Phenol	0.20 mmol/L	80% degradation in 2h under visible light	[5]
6.	0.5% wt.	Acetone and NO	Acetone:1000 ppb and Nitric oxide: 500 ppb	The degradation of acetone and NO under visible light reach up to 38% and 98% respectively in 3h.	[6]

3.2 Materials and methods:

3.2.1 Chemicals Used:

The chemicals employed in the preparation of TiO_2 nanoparticles are as follows. TiO_2 powder with a purity of 99%, ammonia sulphate GR [$(NH_4)_2SO_4$], sulfuric acid (H_2SO_4) 98%, liquor ammonia sp. gr. is 0.91 (about 30% NH_3), lanthanum nitrate with a purity of 99%, citric acid monohydrate GR ($C_6H_8O_7H_2O$), MB dye and Nitric acid GR (HNO_3). All of the above chemicals were acquired from Merck, India.

3.2.2 Synthesis of doped TiO_2 nanoparticles:

The doped TiO_2 crystalline nanoparticles were synthesized by solution-combustion process from TiO_2 powder in a similar manner as reported earlier [7–10]. The process is described for 1 mol % La doping. The 4.7289 g of TiO_2 was dissolved in 100 mL of sulphuric acid, and six times mol of TiO_2 ammonium sulphate was added. The resulting solution was heated with the hot plate using a magnetic bead at about 400 rpm for 2-3 h at a temperature of 180°C, which resulted in titaniumoxysulphate, $TiO(SO_4)$. In another beaker, lanthanum nitrate (0.000626 mol) was added to 50 mL sulfuric acid for 1% La doping, and for other La doping, the $La(NO_3)_3$ amount was added according to stoichiometry. The hot plate was used to heat the resulting solution with the help of magnetic stirrer at about 300 rpm for 2-3 h at 170°C. Then both solutions were mixed hot and cooled to ambient and using distilled water made up to 500 mL of total volume. Then ammonia (NH_3) solution was added gradually so that a white residue was obtained, which was separated through the Buchner funnel. This residue was mixed with 100 mL of HNO_3 to form titanium oxynitrate, $TiO(NO_3)_2$. About 10 g of complexing agent, i.e., monohydrate citric acid, was added, and the total solution was made up to 500 mL by adding double-distilled water. After that, the entire contents were evaporated over a hot plate at 70-80°C with steady stirring till self-ignition occurred. Ignition took place in an

open atmosphere at ambient temperature, and burning occurred by self-promulgating combustion, evacuating significant gases and forming a fluffy brown mass of La-doped TiO_2 that was crushed into powder with a pestle and mortar. Citric acid is utilised as a complexing agent, forming a complex with cations and acting as fuel for the combustion process in the ignition step. The temperature was uplifted by the ignition stage, which resulted in the formation of crystalline powder at a low temperature. The powdered La-doped TiO_2 product was calcined in the presence of the air for 5 h at 500°C. This resulted in the final TiO_2 nanoparticles doped with La. One of the key reasons for using monohydrate citric acid is its environmental friendliness and ease of degradation. Citric acid belongs to the group of organic acids that are easier to degrade and are considered more environmentally friendly than some synthetic chelating agents like EDTA and DPTA [11].

3.2.3 Characterisations:

Employing XRD analysis with Cu-K irradiation (Rigaku Ultima IV, Japan), the average particle size and phase of the obtained undoped and La-doped TiO_2 (with 0.005, 0.01, 0.015, 0.02, and 0.025%) nanoparticles were examined. When determining the bandgap energies of the synthesised photocatalysts, the Kubelka-Munk method was used to analyse the data from the DRS analysis (CORY 100 Bio UV spectrophotometer) using barium sulphate as the reference. The Nicholet 5700 (Thermo Electron) FTIR spectrophotometer was used to record the infrared spectra using the KBr pellet method. Using monochromated Mg-K (1253.6 eV) as the X-ray source (AMICUS, Kratos Analytical, England), the XPS analysis was performed to determine the chemical state and binding energy of elements contained in the produced photocatalysts. XPSPEAK41 and Image- J software was used to analyse XPS and FESEM data, respectively. All the graphs were plotted using Origin 2019b software.

3.2.4 Methodology of kinetic study:

100 mL of the dye solution was introduced into quartz tube of the UV-PCR for dye degradation kinetics analysis, and 0.01 g of prepared nanoparticles was added to this tube. After inserting magnetic bead, the tube was put inside the UV-PCR to allow the dye to be photodegraded. The dye starts to photodegrade as soon as the UV PCR lamp was switched on. Constant stirring was used to comprehensively mix the dye solution and photocatalyst during the photocatalytic process. A 2 mL sample was collected from the tube after every 5 min and centrifuged for 2 min before measuring its concentration. The same procedure was used with all catalysts. The different catalysts prepared with La doping (0, 0.5, 1, 1.5, 2.0 and 2.5 %) were used and dye concentrations in solution were 10, 20, 30, 40 and 50 ppm. For comparison of catalysts, the kinetic studies with commercial TiO_2 nanoparticles Aeroxide P-25 (bought from Sigma Aldrich) were also carried out.

3.3 Results and discussion

3.3.1 XRD:

X-ray diffraction was used to understand the consequence of various percentages of La doping in TiO_2 and investigate the crystal structure. In Figure 3.1, XRD plots for undoped TiO_2 and doped TiO_2 have been shown. All the prepared nanoparticles have anatase phase without any significant rutile phase [12].

Figure 3.1 shows XRD patterns of both undoped and La-doped TiO_2 nanoparticles. The peak at the 2θ (25.351) corresponds to plane alter the structure of TiO_2 as it remains 101 of anatase phase. Meanwhile, Lanthanum ionic radius has the value of 1.03Å which is greater than that of Titanium, which has a value of 0.62Å, so it can't replace the Ti ion and leftovers at interstitials of Titanium dioxide beneath the range of scan of XRD. So, these dissimilarities between La and Ti ions radii may create bonds of Ti-O-La or lanthanum oxide (La_2O_3) at the anatase surface relative to actual assimilation of La^{3+} in

the lattice of the TiO_2. The La_2O_3 peak is not present in the XRD plot because it is scattered and can't be discovered in the XRD pattern [14]. It is also evident from Figure 3.1 that on increasing doping percentage of La, the intensities of prepared samples also increase significantly. With a rising La percentage of doped nanoparticles, notably for anatase phase, values of crystallite size of synthesized La-doped TiO_2 samples significantly diminish and recombine capacity of pairs of electron-hole on excitation of La^{3+} on TiO_2 is inhibited, promoting the activity of photocatalysis of prepared photocatalysts [14].

The average crystallite size of TiO_2 and 1.5 % La-doped TiO_2 was found to be 30.16 and 19.90 nm. respectively. A similar result would also be found by Lan et al. [24].

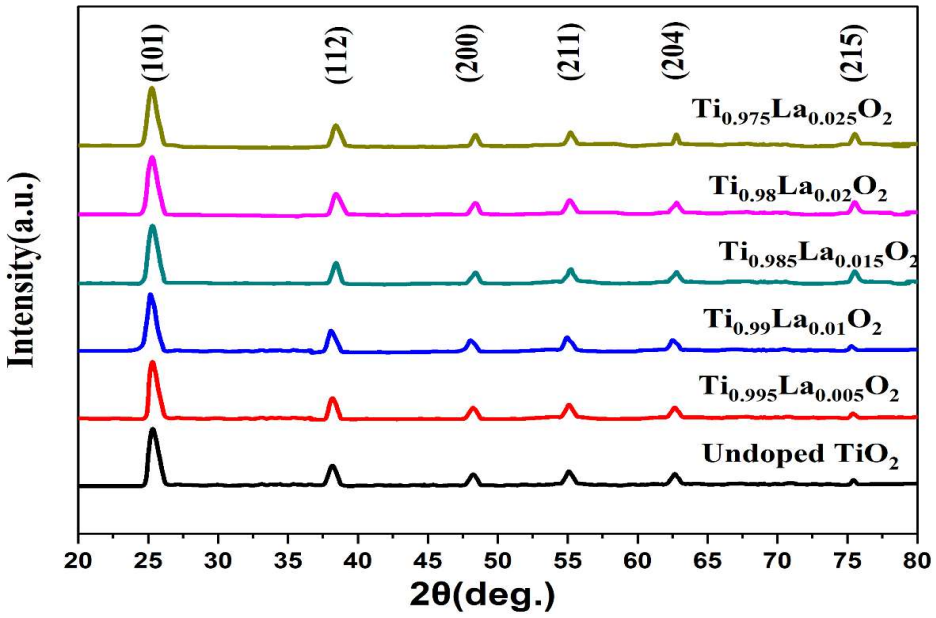

Figure 3.1 XRD diagram of La-doped and undoped TiO_2 photocatalysts

3.3.2 FTIR:

Fourier Transform Infrared Spectroscopy was applied to detect distinct functional groups in the lanthanum-doped and undoped TiO_2 photocatalysts. The FTIR spectra presented in

Figure 3.2 show the stretching vibrations of OH functional group at the wavenumber of 3450 cm^{-1}. All the La-doped and undoped photocatalysts peak at the wavenumber of 1020 cm^{-1}, which relates to the anatase phase of Ti-O vibrations. Undoped TiO_2 shows a band at the wavenumber of 512 cm^{-1}, a characteristic peak of TiO_2, but with doped TiO_2 with La, this characteristic peak shifts at 480 cm^{-1}, which might correspond to bond structure of Ti-O-La. Sibu et al. [16] also reported these results in a similar range. This shift in the peak position reflects the changes in the bond lengths and angles within the TiO_2 structure, as the larger ionic radius of La^{3+} ion [17]. The shift in the FTIR peak from 512 cm^{-1} to 480 cm^{-1} lead to the formation of additional energy levels within the band gap, which can facilitate the separation of photogenerated electron-hole pairs and enhance the photocatalytic efficiency [18]. The band spectra situated at the wavenumber of 1620 cm^{-1} validate the occurrence of OH groups at photocatalysts' surface, also called bending vibrations of the water (H-O-H bending) molecules which are absorbed at the surface of nanoparticles. Nie et al. and Coromelci et al. [18,19] also reported occurrence of OH group and vibrations of water molecules in similar range.

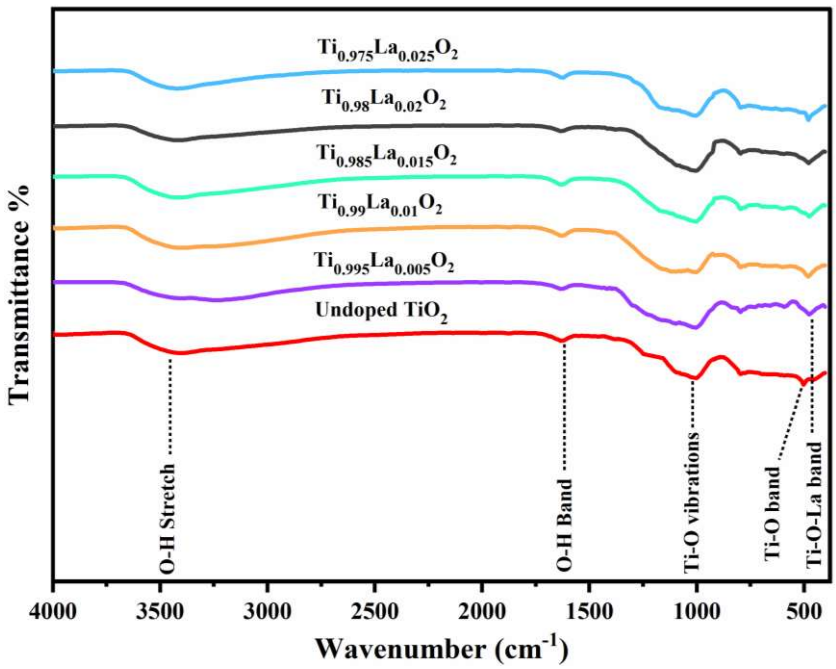

Figure 3.2 FTIR plots of La-doped and undoped TiO_2 photocatalysts

3.3.3 DRS:

The optical absorbance spectra of synthesized TiO_2 doped with La and bare TiO_2 was measured in the UV–Visible range and is presented in Figure 3.3.

It is noticeable from inset of Figure 3.3 that band gap values of prepared nanoparticles are decreased from 3.2 eV to 2.7 eV on rising doping percentages of lanthanum from 0 to 2.5 %. Nie et al. also reported a decrease in band gap values on increasing La doping in TiO_2 photocatalysts [19].

Results show that metals addition into TiO_2 photocatalysts causes a slight reduction in band-gap values. This variation in band-gap values may be the result of the dielectric confinement effect. The occurrence of this type of band corresponds to the displacement of charge to conduction band from valence band of TiO_2 (because of 2p orbital of oxygen). Due to the fact that the dielectric constant of La_2O_3 is lower than that of TiO_2, the energy change brought on by dielectric confinement (due to doping of La) is more significant than that brought on by the impact of space limitations on electron holes and which is evident from the decrease in band-gap values is therefore detected that is known as Red-shift [20].

3.3.4 FE-SEM:

FE-SEM was used to conduct the morphological and microstructural analysis of the prepared bare and La-doped photocatalysts. In Figure 3.4, FE-SEM images of the prepared photocatalysts bare and 1.5% La-doped TiO_2 are shown. From these pictures, it is evident that photocatalysts are of spherical shape. It is also clear from these figures that the morphology of doped photocatalysts remains unchanged, and some agglomeration may be due to the magneto-dipole interaction. It is also accomplished that doped photocatalysts' particle size is decreased compared to undoped one, having sizes approximately 22.24 and 32.28 nm, respectively. It agrees with the XRD data. This is

beneficial because when size of the particle is decreased, surface area is increased, which enhances photocatalytic sites, which eventually increases photocatalytic activity of prepared samples [19–22].

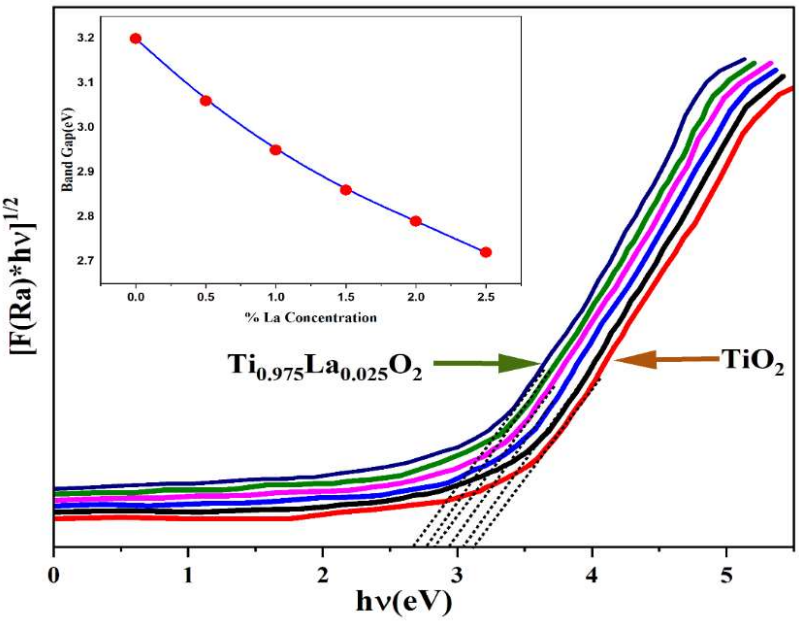

Figure 3.3 DRS plots of La-doped and undoped TiO_2 photocatalyst

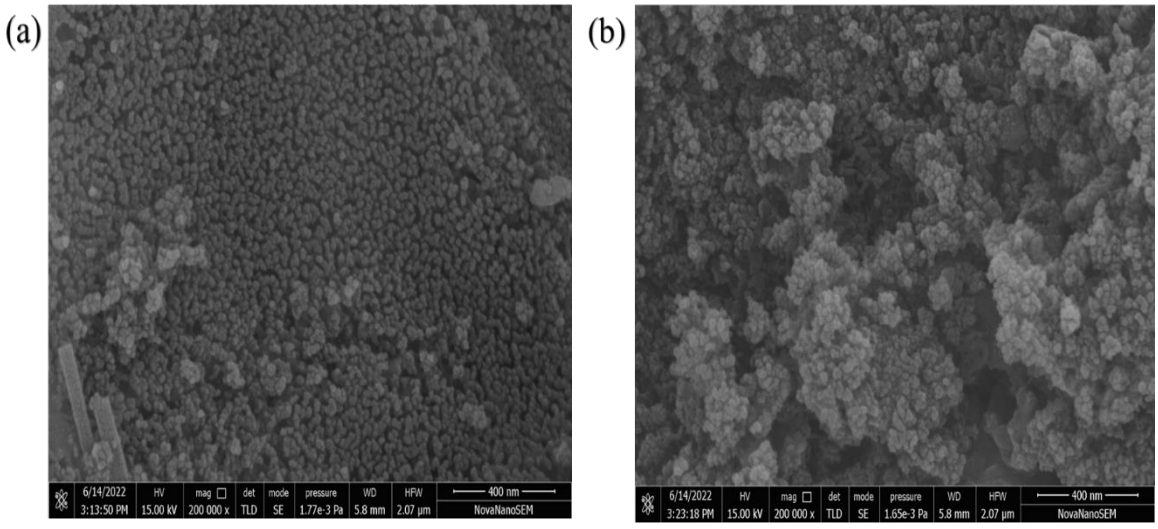

Figure 3.4 FE-SEM Pictures of (a) undoped (b) 1.5% La-doped TiO_2 Photocatalysts

3.3.5 XPS:

The XPS was applied to analyse the composition of elements present at the surface and the chemical oxidation state of nanoparticles [22]. Figure 3.5 (a) represents the full scan spectra which confirms the presence of O and Ti elements on the bare TiO_2's surface and presence of O, Ti and La on 1.5% doped TiO_2's surface.

In Figure 3.5 (b), XPS spectra of 2p orbital of Ti is represented in doped TiO_2 and 1.5% La-doped TiO_2. Both doped and undoped samples show two noticeable peaks attributed to Ti $2p_{3/2}$ and Ti $2p_{1/2}$, respectively, indicating that the normal tetravalent oxidation state of titanium predominates Ti^{4+} in anatase TiO_2 [24]. The binding energy of undoped TiO_2 sample is 458.6 and 464.4 eV. After doping of La 1.5% binding energy increases by 0.2 eV and peaks shifts to higher values which shows the existence of various electronic interactions amid Ti and oxides of La because of their difference in electronegativity, which lowers Titanium external electron density and therefore raises Ti 2p's binding energy [25].

In Figure 3.5 (c) XPS plot of undoped TiO_2 for O 1s is shown. The peaks at binding energy of 529.3 eV and 531.1 eV are accredited to lattice oxygen and OH group, respectively, in undoped TiO_2 samples. In Figure 3.5 (d) XPS plot for 1.5% La-doped TiO_2 has been shown for O 1s in which two peaks are observed at the binding energy of 529.5 eV and 531.3 eV, which are more than that of 0.2 eV and a third peak is shown at the binding energy of 532.3 eV, which corresponds to the La-O bond and is further confirmed by FTIR analysis. Figure 3.5 (e) depicted the La 3d spectrum of 1.5% La-doped TiO_2. In this figure, the peaks endorsed to the spin split orbit La $3d_{3/2}$ and La $3d_{5/2}$ levels, indicating that the presence of La^{3+} species is represented at 853.2 and 836.5 eV. respectively [1]. In the literature, binding energies values of 3d shift of La are given as 851.8 eV and 834.9 eV, but here, it is found that these values shift to greater energy levels.

This is possible because of the replacement of Ti^{4+} by La^{3+}, so it is clear that there is no incorporation of La in TiO_2's lattice rather than in the configuration of Ti-O-La bond [5,26,27]. The reason for shifting binding energies in doped TiO_2 is that La is less electronegative than Ti, so charge disparity occurs. As a result, the binding energy alters, and the La electron density in the Ti-O-La decreases [28].

As described earlier in Figure 3.5 (d) that the presence of La–O bond can confirm the dopant La have not entered the lattices. The oxygen vacancies for charge compensation can be caused by the progress of the acceptor La^{3+} ions into TiO_2 [14] as following:

$$La_2O_3 \xrightarrow{TiO_2} 2La'_n + V_o^{\cdot\cdot} + 3O_o \qquad 3.1$$

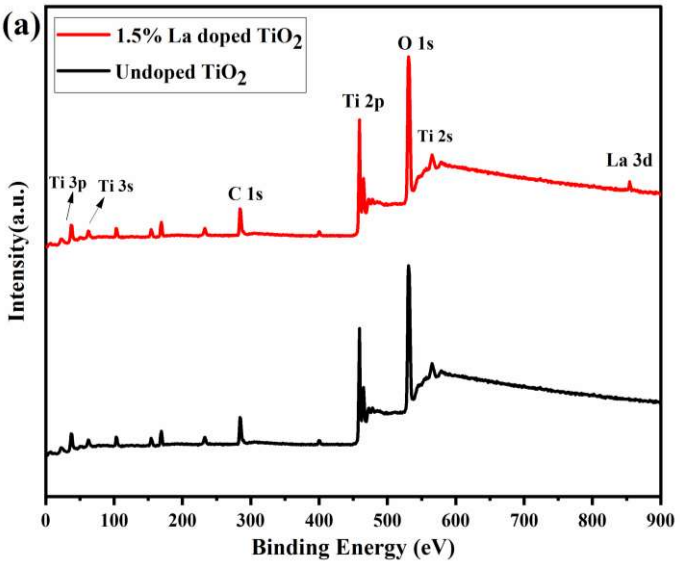

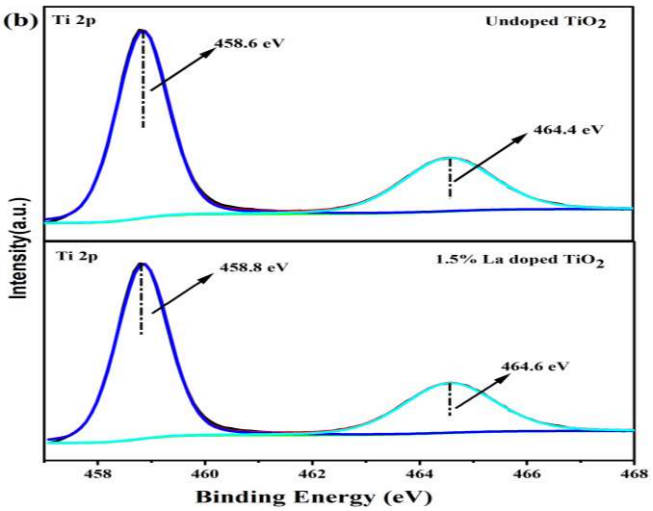

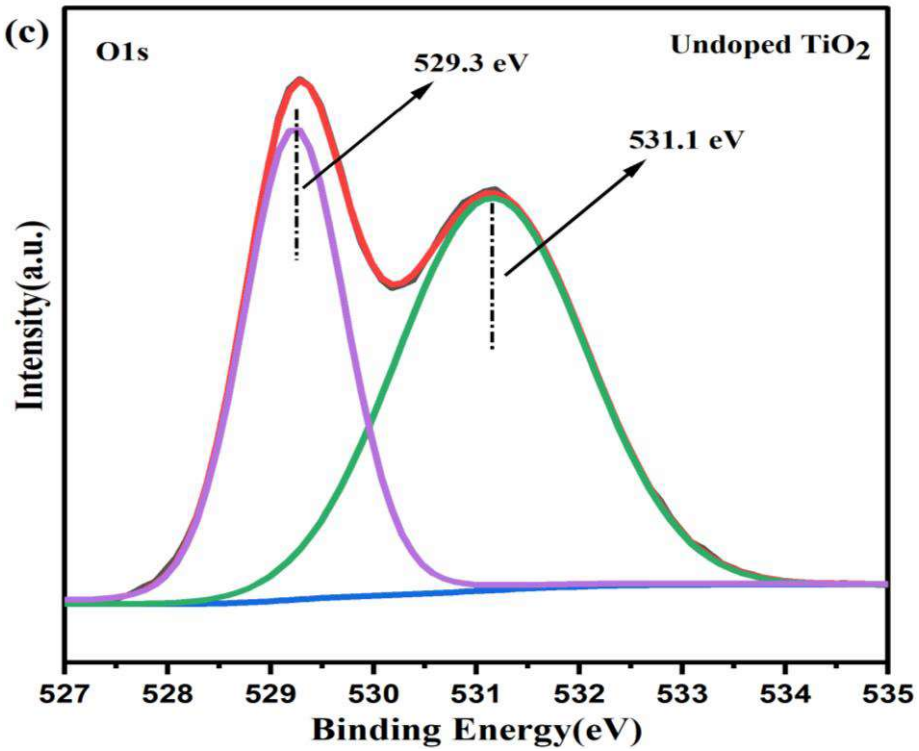
(c)
O1s
Undoped TiO2
529.3 eV
531.1 eV
Intensity(a.u.)
527
528
529
530
531
532
533
534
535
Binding Energy(eV)

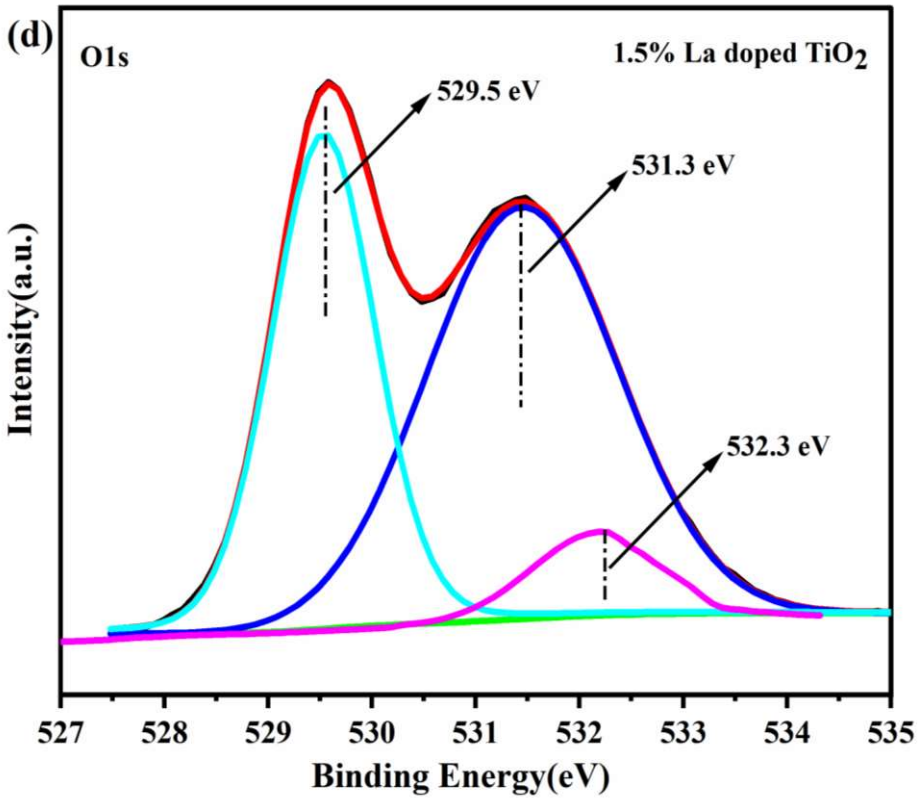
(d)
O1s
1.5% La doped TiO2
529.5 eV
531.3 eV
532.3 eV
Intensity(a.u.)
527
528
529
530
531
532
533
534
535
Binding Energy(eV)

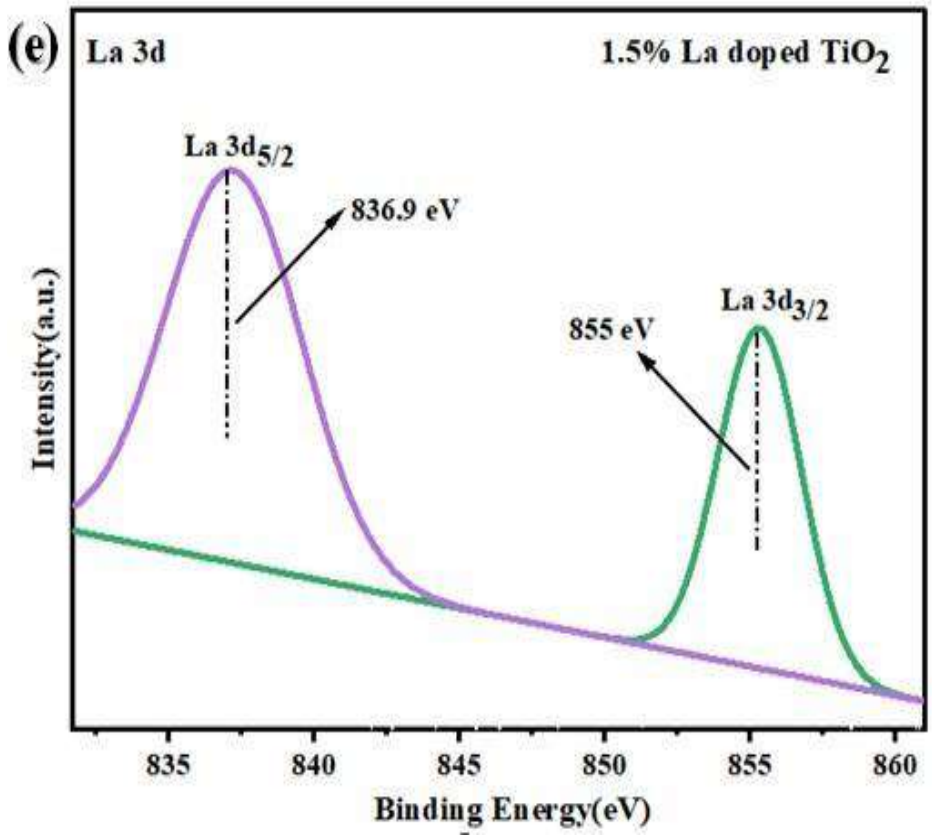

Figure 3.5 XPS spectra of (a) Total spectra for TiO_2 and 1.5% La doped TiO_2 (b) fitting curves of the Ti 2p regions (c) fitting curve of O 1 s region of undoped TiO_2 (c) fitting curve of O 1 s region of 1.5% La doped TiO_2 (e) fitting curves of La 3d regions

3.3.6 Mechanism

Photocatalytic activity of undoped and La-doped TiO_2 nanoparticles was determined by measuring the variation of concentration due to degradation of MB dye solution during photocatalysis in UV- PCR. First, it is well acknowledged that doping with La is likely to develop an oxygen vacancy. The oxygen vacancy may then operate like a trapper to prevent pairs of electrons and holes from recombining, which are photo-generated [29]. Additionally, Wu et al. [30] revealed that when La is doped in TiO_2, it can convert Ti^{4+} to Ti^{3+} via charge compensation. La doping may cause impurity levels due to coaction of Ti^{3+} and oxygen vacancies, which might prevent charge carriers from combining. The

other benefit of photocatalytic activity is that La_2O_3 on surface of TiO_2 might move electrons onto the surface. The space charge area gets smaller, and the surface barrier increases as the dopant percentage (La) increases. Additionally, the depth of light penetration into titania significantly surpasses space charge film when the dopant percentage is too prominent. Space charge area becomes quite constrained; as a result, it is simpler to recombine the photogenerated electron-hole pairs [27].

When a photon of appropriate energy is incident on photocatalyst, the electrons are ejected, leaving behind holes. The electrons combine with oxygen to form superoxide. This superoxide radical and holes combine with H_2O to give $OH^{\cdot}$ radicals [31,33]. The radicals $O2^{-\cdot}$ and $OH^{\cdot}$ are highly reactive and oxidise and degrade the organic dyes in the simpler inorganic products [33,34]. The different equations have been discussed by Raza et al. [35] which shows the production of $OH^{\cdot}$ radical leads to degradation of dye.

These equations are given below:

$$TiO_2 \text{ (doped)} + h\nu \longrightarrow TiO_2 (h^+_{vb} + e^-_{cb}) \quad 3.2$$

$$O_2^- + e_{cb}^- \rightarrow O_2^{-\cdot} \quad 3.3$$

$$OH^{\cdot} / O_2^{-\cdot} + \text{dyes} \rightarrow CO_2 + H_2O \quad 3.4$$

$$H_2O + h^+_{vb} \rightarrow H^+ + OH^{\cdot} \quad 3.5$$

3.3.7 Kinetics study La-doped TiO_2:

All the catalysts' kinetic analysis were completed, and Figure 3.6 and Figure 3.7 depicts kinetic data for degradation of MB dye in its aqueous solution with 1.5% La-doped TiO_2 photocatalyst. The data were analysed by pseudo first order kinetics given by Eq. 3.6 and solving it gives $-\ln (C/Co) = -k_pC$, where C is concentration at time t and Co is the initial concentration and k_p is rate constant.

$$-dC/dt = k_p C \qquad 3.6$$

The reaction rate constant k_p for degradation of MB dye of the undoped and La-doped TiO_2 photocatalyst are given in Table 3.2 along with R^2 values. The reaction rate was found to increase significantly using TiO_2 doped with La as compared to undoped TiO_2. TiO_2 doped with 1.5 % La has the maximum reaction rate constant, which is consistent with other results [1].

Table 3.2 Summary of the degree of fitting (R^2) and reaction rate constants of the undoped and La-doped TiO_2 photocatalysts.

	10 ppm		**20 ppm**		**30 ppm**		**40 ppm**		**50 ppm**	
Catalyst	k_p	R^2	k_p	R^2	k_p	R^2	k_p	R^2	k_p	R^2
Undoped TiO_2	0.035	0.988	0.036	0.981	0.035	0.973	0.036	0.993	0.039	0.989
$Ti_{0.995}La_{0.005}O_2$	0.041	0.980	0.038	0.971	0.038	0.981	0.037	0.962	0.041	0.995
$Ti_{0.990}La_{0.010}O_2$	0.044	0.981	0.045	0.973	0.041	0.967	0.040	0.995	0.042	0.991
$Ti_{0.985}La_{0.015}O_2$	0.046	0.983	0.046	0.980	0.048	0.995	0.046	0.970	0.047	0.969
$Ti_{0.980}La_{0.020}O_2$	0.045	0.982	0.046	0.986	0.042	0.974	0.045	0.986	0.045	0.982
$Ti_{0.975}La_{0.025}O_2$	0.045	0.981	0.045	0.994	0.039	0.952	0.042	0.989	0.042	0.939

k_p is in min^{-1}.

The current results are comparable to various previous literature given in Table 3.3.

Table 3.3 Comparison of photocatalytic activity of various Photocatalysts with different pollutants

Dopant	Optimum doping	Pollutant	Light source	Time (min)	Degradation efficiency (%)	Ref.
Sn	5 % mol	MB	125 W Hg lamp	120	77	[36]
Ag	0.5% mol	Methyl Orange	500 W Xe lamp	180	52.1	[37]
Gd	0.3 % mol	Methyl Orange	500 W Hg lamp	28	50	[38]
Fe	1.5 % mol	2,4 D	Mercury lamp of 15 watts	120	65	[39]
Fe-N	1% Fe & % N mol	MB	25 W fluorescent lamp	300	80.5	[40]
La-V	10 % V and 5 % La mol	Methyl Orange	Xenon lamp Reactor 500 W	180	70	[41]
La	1.5 % mol	MB	UV Photo-chemical Reactor with 8W 8 tubes	40	88.71	Present Work

It is impressive that the rate of MB's photocatalytic degradation first rises with an increased doping percentage of La before showing a reversal pattern after the amount of La reaches its optimum level. The space charger zone became small, which helped photogenerated pairs of electrons and holes separate effectively. As the percentage of La surged, specialized surface area expanded, and obstructions to the surface improved. The space charge area becomes extremely small when the percentage of La is very high, which might enable light to penetrate titania much deeper than the space charge layer. As a result, it is simpler to recombine for photo-generated charge carriers, and the photocatalytic activity would be decreased [26].

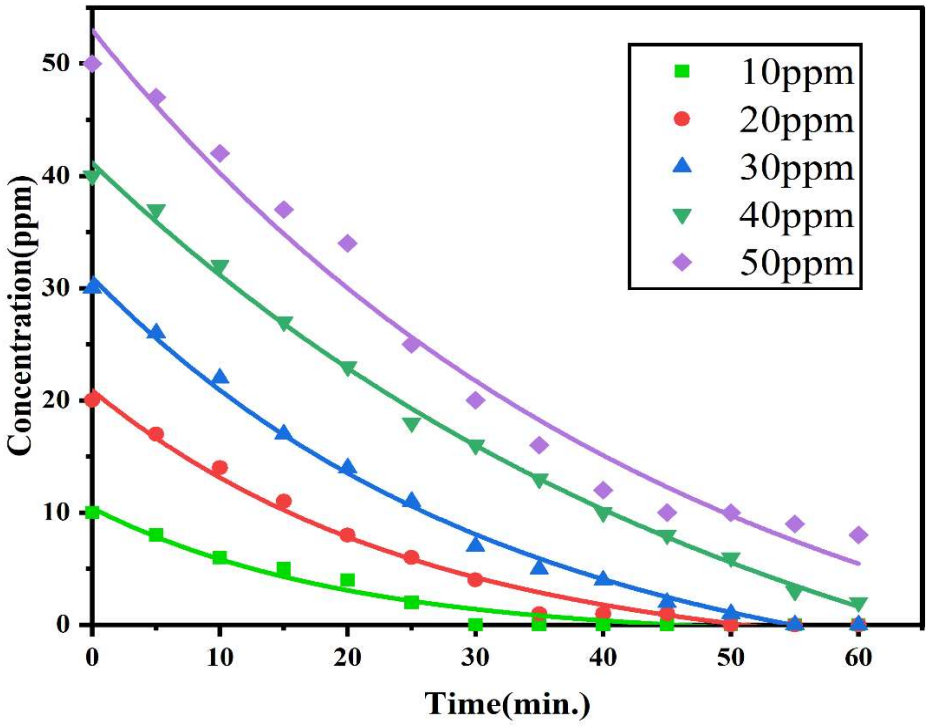

Figure 3.6 Variation of initial concentration of MB during degradation with time with $Ti_{0.985}La_{0.015}O_2$ photocatalyst

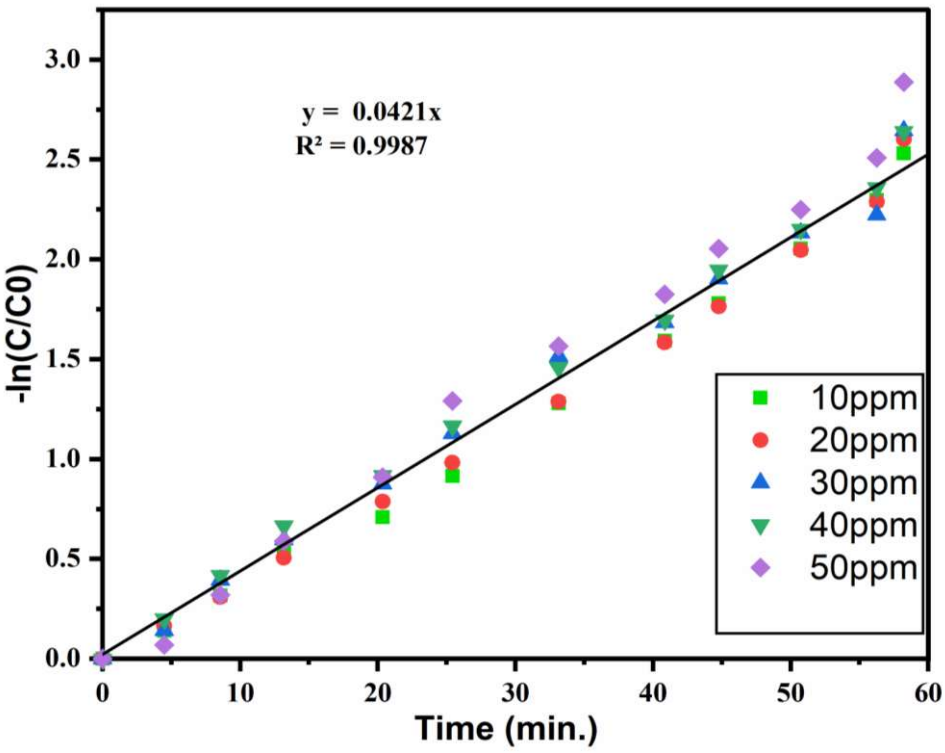

Figure 3.7 Kinetic analysis of degradation of MB dye by $Ti_{0.985}La_{0.015}O_2$ photocatalyst, -ln(C/Co) vs t data

According to an adsorption investigation of the dye on the nanoparticles, only 1-2% of the dye was retained on the photocatalyst's surface. A negligible amount of the dye was photodegraded when no photocatalysts were present in the UV light source.

The reusability of photocatalysts is vital for industrial applications and economy. Figure 3.8 shows the results of the successive reusability experiments with best photocatalyst (1.5% La-doped TiO_2) performed for five cycles. Figure 3.8 reveals that degradation in 40 min continuously decreases (85.72% to 77.87%) from first to fifth cycle however with fresh catalyst degradation was 88.71%. So, there is a very small reduction in degradation efficiency (7.85%) after fifth cycle. It is also evident from Figure 3.8 that the shape of all the curves is almost similar. The above analysis concludes that 1.5% La-doped TiO_2 is highly stable throughout the photocatalytic degradation of MB dye.

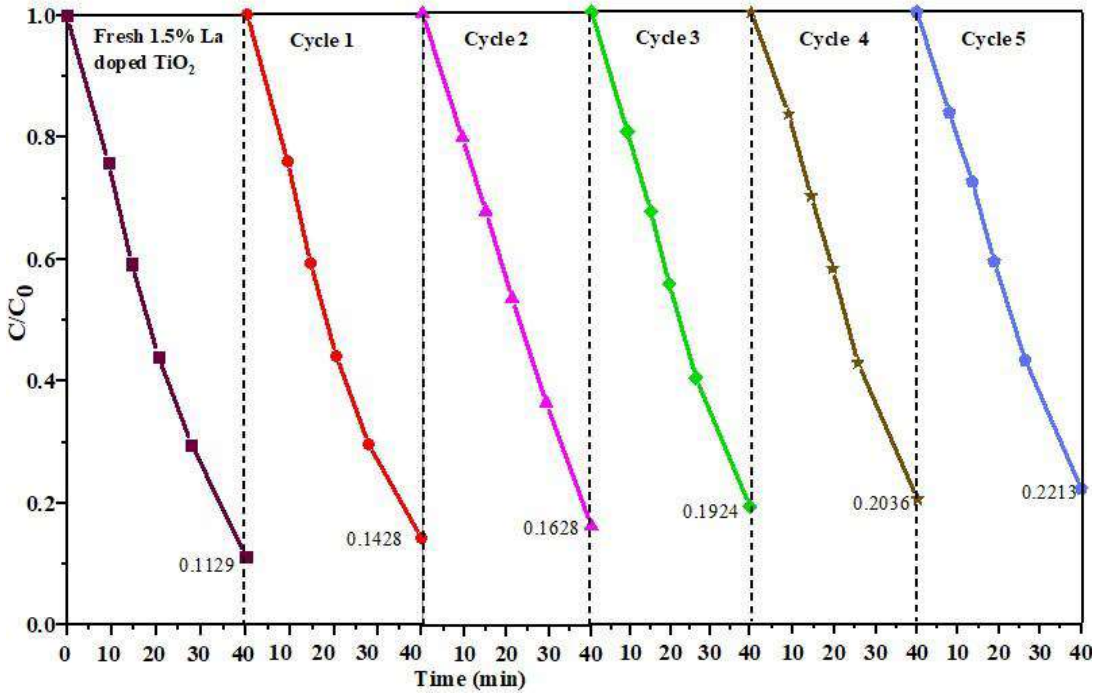

Figure 3.8 The reusability of 1.5% La-doped TiO_2 for the breakdown of MB dye at 30 ppm

Figure 3.9 displays the pictographic representation of photocatalytic breakdown of the MB dye of 30 ppm with 0.01g of photocatalyst $Ti_{0.985}La_{0.015}O_2$ in UV-PCR at the time interval of 5 min. Here in this sample 1, 2, 3,……10 represents MB concentration after time at 0, 5, 10,…….45 min respectively.

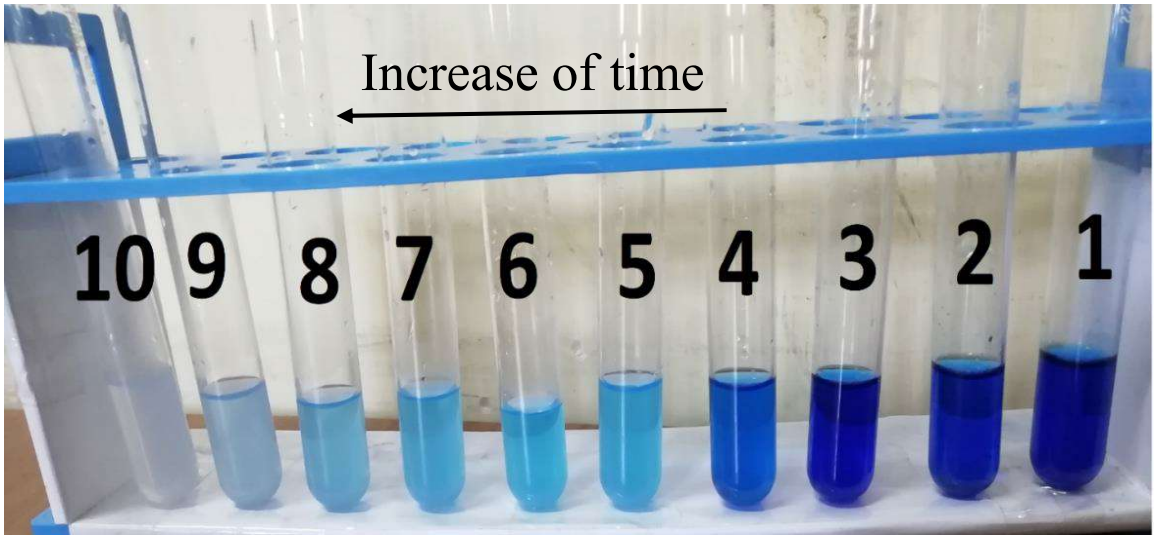

Figure 3.9 Pictographic depiction of degradation of MB dye of initial concentration 30 ppm in aqueous solution in UV-PCR reactor using 0.01g $Ti_{0.985}La_{0.015}O_2$ photocatalyst

3.3.8 Comparison among the best doped photocatalyst ($Ti_{0.985}La_{0.015}O_2$), undoped TiO_2, and Aeroxide P-25

Aeroxide P-25 and the best-doped TiO_2 sample, $Ti_{0.985}La_{0.015}O_2$, as well as the prepared undoped TiO_2 were compared; the results are given in Figure 3.10. The results show that the TiO_2 doped with 1.5% La ($Ti_{0.985}La_{0.015}O_2$) displayed the best photocatalytic performance. The doping of La could reduce the bandgap hence providing a potential to use more part of solar spectrum for degradation of pollutants and also it can be used in solar cells for future research.

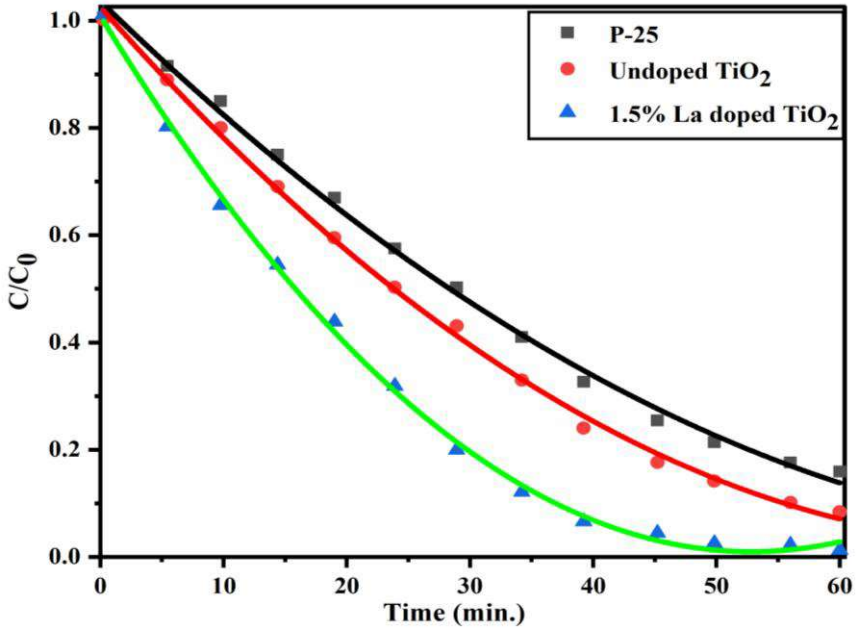

Figure 3.10 Comparison of the best photocatalyst among undoped TiO_2, $Ti_{0.985}La_{0.015}O_2$ and Aeroxide P-25 for degradation of the MB dye of initial concentration 30 ppm

3.4 Conclusion:

TiO_2 and La-doped [$LaTi_{1-x}La_xO_2$ (x = 0.00-0.025)] nanoparticles could be prepared by solution-combustion process. The prepared nanoparticles were characterised by XRD, FTIR, FE-SEM, DRS and XPS. Photocatalytic performance of each prepared bare and doped TiO_2 photocatalyst was assessed using UV-PCR. The kinetic investigations of all catalysts show that 1.5% La-doped TiO_2 nanoparticles have the best activity for the photocatalysis process in the UV-PCR reactor midst all the synthesized photocatalysts. The current study also discovered that as soon as the La concentration rises to 1.5%, so does activity of TiO_2 to photodegradation; however, the photocatalytic activity begins to diminish after doping concentration increases beyond 1.5%. At 1.5% La doping, TiO_2 had the maximum photocatalytic activity. The results of a comparative investigation between synthesised undoped TiO_2, 1.5% La-doped TiO_2, and Aeroxide P-25 photocatalysts demonstrate that the synthesised 1.5% La-doped TiO_2 photocatalyst outperforms the

undoped TiO_2 and P-25 photocatalysts. The utilised photocatalyst ($Ti_{0.985}La_{0.015}O_2$) was reused after regeneration for five times to degrade MB dye; the reuse makes photodegradation process more economical. The results of the photodegradation indicate that the $Ti_{0.985}La_{0.015}O_2$ photocatalyst's performance diminishes with the number of reuses, after fifth cycle a loss of only 7.85% of activity was there.

References

[1] M. Han, Z. Dong, J. Liu, G. Ren, M. Ling, X. Yang, L. Zhang, B. Xue, F. Li, The role of lanthanum in improving the visible-light photocatalytic activity of TiO_2 nanoparticles prepared by hydrothermal method, Appl. Phys. A Mater. Sci. Process. 126 (2020) 1–10. https://doi.org/10.1007/s00339-020-04135-8

[2] K. Dai, T. Peng, H. Chen, J. Liu, L. Zan, Photocatalytic degradation of commercial phoxim over la-doped TiO_2 nanoparticles in aqueous suspension, Environ. Sci. Technol. 43 (2009) 1540–1545. https://doi.org/10.1021/es802724q

[3] Y. Huang, J.J. Cao, F. Kang, S.J. You, C.W. Chang, Y.F. Wang, High selectivity of visible-light-driven la-doped TiO_2 photocatalysts for NO removal, Aerosol Air Qual. Res. 17 (2017) 2555–2565. https://doi.org/10.4209/aaqr.2017.08.0282

[4] H. Lee, J. Park, S.S. Lam, Y.K. Park, S.C. Kim, S.C. Jung, Diclofenac degradation properties of a La-doped visible light-responsive TiO_2 photocatalyst, Sustain. Chem. Pharm. 25 (2022) 100564. https://doi.org/10.1016/j.scp.2021.100564

[5] J. Liqiang, S. Xiaojun, X. Baifu, W. Baiqi, C. Weimin, F. Honggang, The preparation and characterization of la doped TiO_2 nanoparticles and their photocatalytic activity, J. Solid State Chem. 177 (2004) 3375–3382. https://doi.org/10.1016/j.jssc.2004.05.064

[6] C.C. Ho, F. Kang, G.M. Chang, S.J. You, Y.F. Wang, Application of recycled lanthanum-doped TiO_2 immobilized on commercial air filter for visible-light photocatalytic degradation of acetone and NO, Appl. Surf. Sci. 465 (2019) 31–40. https://doi.org/10.1016/j.apsusc.2018.09.136

[7] S. Saroj, L. Singh, S.V. Singh, Solution-combustion synthesis of anion (iodine) doped TiO_2 nanoparticles for photocatalytic degradation of Direct Blue 199 dye and regeneration of used photocatalyst, J. Photochem. Photobiol. A Chem. 396 (2020) 112532. https://doi.org/10.1016/j.jphotochem.2020.112532

[8] S. Saroj, L. Singh, S.V. Singh, Photodegradation of Direct Blue-199 in carpet industry wastewater using iron-doped TiO_2 nanoparticles and regenerated photocatalyst, Int. J. Chem. Kinet. 51 (2019) 189–205. https://doi.org/10.1002/kin.21243

[9] Madhvi, L. Singh, S. Saroj, Y. Lee, S.V. Singh, Facile synthesis of nano-crystalline

anatase TiO_2 and their applications in degradation of Direct blue 199, J. Mater. Sci. Mater. Electron. 27 (2016) 2581–2588. https://doi.org/10.1007/s10854-015-4061-5

[10] S. Saroj, L. Singh, R. Ranjan, S.V. Singh, Enhancement of photocatalytic activity and regeneration of Fe-doped TiO_2 ($Ti_{1-x}Fe_xO_2$) nanocrystalline particles synthesized using inexpensive TiO_2 precursor, Res. Chem. Intermed. 45 (2019) 1883–1906. https://doi.org/10.1007/s11164-018-3708-2

[11] M.A. Budihardjo, B.S. Ramadan, R.P. Safitri, A.J. Effendi, S. Hidayat, Y.V. Paramitadevi, B. Ratnawati, Metals Removal from Contaminated Soil Using Electrokinetic Treatment – Effect of Different Permeable Reactive Barrier and Flushing Solution, Ecol. Eng. Environ. Technol. 24 (2023) 19–27. https://doi.org/10.12912/27197050/156969.

[12] Z. Shi, X. Zhang, S. Yao, Preparation and photocatalytic activity of TiO_2 nanoparticles co-doped with Fe and la, Particuology 9 (2011) 260–264. https://doi.org/10.1016/j.partic.2010.05.017

[13] Z.N. Kayani, Maria, S. Riaz, S. Naseem, Magnetic and antibacterial studies of sol-gel dip coated Ce doped TiO_2 thin films: Influence of Ce contents, Ceram. Int. 46 (2020) 381–390. https://doi.org/10.1016/j.ceramint.2019.08.272

[14] P. Pascariu, C. Cojocaru, M. Homocianu, P. Samoila, A. Dascalu, M. Suchea, New La^{3+} doped TiO_2 nanofibers for photocatalytic degradation of organic pollutants: Effects of thermal treatment and doping loadings, Ceram. Int. 48 (2022) 4953–4964. https://doi.org/10.1016/j.ceramint.2021.11.033

[15] C.P. Sibu, S.R. Kumar, P. Mukundan, K.G.K. Warrier, Structural modifications and associated properties of lanthanum oxide doped sol-gel nanosized titanium oxide, Chem. Mater. 14 (2002) 2876–2881. https://doi.org/10.1021/cm010966p

[16] C. Coromelci, M. Ignat, L. Sacarescu, M. Neamtu, Enhanced visible light activated mesoporous titania by rare earth metal doping, Microporous Mesoporous Mater. 341 (2022) 112072. https://doi.org/10.1016/j.micromeso.2022.112072

[17] J. Li, M. Yao, Y. Zhang, nano-composite films, 16 (2009) 315–321.

[18] P. Sanjay, E. Chinnasamy, K. Deepa, J. Madhavan, S. Senthil, Synthesis, Structural, Morphological and Optical Characterization of TiO2 and Nd3+ Doped TiO2 Nanoparticles by Sol Gel Method: A Comparative Study for Photovoltaic Application, IOP Conf. Ser. Mater. Sci. Eng. 360 (2018). https://doi.org/10.1088/1757-899X/360/1/012011.

[19] J. Nie, Y. Mo, B. Zheng, H. Yuan, D. Xiao, Electrochemical fabrication of lanthanum-doped TiO_2 nanotube array electrode and investigation of its photoelectrochemical capability, Electrochim. Acta 90 (2013) 589–596. https://doi.org/10.1016/j.electacta.2012.12.049

[20] A. Bashir, F. Bashir, M. Sultan, M. Mubeen, A. Iqbal, Z. Akhter, Influence of nickel and lanthanum ions co-doping on photocatalytic properties of TiO_2 for effective degradation of reactive yellow 145 in the visible region, J. Sol-Gel Sci. Technol. 93 (2020) 438–451. https://doi.org/10.1007/s10971-019-05162-5

[21] D.S. Mathew, R.S. Juang, An overview of the structure and magnetism of spinel ferrite nanoparticles and their synthesis in microemulsions, Chem. Eng. J. 129 (2007) 51–65. https://doi.org/10.1016/j.cej.2006.11.001

[22] Y. Köseoɔlu, Structural and magnetic properties of Cr doped NiZn-ferrite nanoparticles prepared by surfactant assisted hydrothermal technique, Ceram. Int. 41 (2015) 6417–6423. https://doi.org/10.1016/j.ceramint.2015.01.079

[23] W. Xue, G. Zhang, X. Xu, X. Yang, C. Liu, Y. Xu, Preparation of titania nanotubes doped with cerium and their photocatalytic activity for glyphosate, Chem. Eng. J. 167 (2011) 397–402. https://doi.org/10.1016/j.cej.2011.01.007

[24] L. Yu, X. Yang, J. He, Y. He, D. Wang, One-step hydrothermal method to prepare nitrogen and lanthanum co-doped TiO_2 nanocrystals with exposed {0 0 1} facets and study on their photocatalytic activities in visible light, J. Alloys Compd. 637 (2015) 308–314. https://doi.org/10.1016/j.jallcom.2015.03.035

[25] X.F. Lei, C. Chen, X. Li, X.X. Xue, H. Yang, Characterization and photocatalytic performance of la and C co-doped anatase TiO_2 for photocatalytic reduction of Cr(VI), Sep. Purif. Technol. 161 (2016) 8–15. https://doi.org/10.1016/j.seppur.2016.01.030

[26] X. Lan, L. Wang, B. Zhang, B. Tian, J. Zhang, Preparation of lanthanum and boron co-doped TiO_2 by modified sol-gel method and study their photocatalytic activity, Catal. Today 224 (2014) 163–170. https://doi.org/10.1016/j.cattod.2013.10.062

[27] Y. Cong, B. Tian, J. Zhang, Improving the thermal stability and photocatalytic activity of nanosized titanium dioxide via La^{3+} and N co-doping, Appl. Catal. B Environ. 101 (2011) 376–381. https://doi.org/10.1016/j.apcatb.2010.10.006

[28] L. Yu, X. Yang, J. He, Y. He, D. Wang, A fluorine free method to synthesize nitrogen and lanthanum co-doped TiO2 nanocrystals with exposed {0 0 1} facets for enhancing visible-light photocatalytic activity, J. Mol. Catal. A Chem. 399 (2015) 42–47. https://doi.org/10.1016/j.molcata.2015.01.022

[29] N. Zhao, M.M. Yao, F. Li, F.P. Lou, Microstructures and photocatalytic properties of Ag and La^{3+} surface codoped TiO_2 films prepared by solgel method, J. Solid State Chem. 184 (2011) 2770–2775. https://doi.org/10.1016/j.jssc.2011.08.014

[30] H.H. Wu, L.X. Deng, S.R. Wang, B.L. Zhu, W.P. Huang, S.H. Wu, S.M. Zhang, The preparation and characterization of la doped TiO_2 nanotubes and their photocatalytic activity, J. Dispers. Sci. Technol. 31 (2010) 1311–1316. https://doi.org/10.1080/01932690903227071

[31] R. Banu, N. Salvi, S. Gupta, C. Ameta, R. Ameta, P.B. Punjabi, A Facile Synthesis of GO/CuO Nanocomposite with Enhancing Photocatalytic Activity for the Degradation of Azure-B Dye and Its Antimicrobial Behavior, Arab. J. Sci. Eng. 47 (2022) 365–378. https://doi.org/10.1007/s13369-021-05421-0

[32] A.S.M. Nur, M. Sultana, A. Mondal, S. Islam, F.N. Robel, A. Islam, M.S.A. Sumi, A review on the development of elemental and codoped TiO_2 photocatalysts for enhanced dye degradation under UV–vis irradiation, J. Water Process Eng. 47 (2022) 102728. https://doi.org/10.1016/j.jwpe.2022.102728

[33] S.A. Jasim, I. Patra, A.M. Abdulhadi, M.E. Al-Gazally, H. Sharma, T. Alawsi, H.T. Mohammed, S.A. Hussein, U.S. Altimari, A.T. Hammid, C. Chem, Magnetic $CeO_2/SrFe_{12}O_{19}$ Nanocomposite: Synthesis, Characterization and Photocatalytic Degradation of Methyl Orange, Arab. J. Sci. Eng. (2022). https://doi.org/10.1007/s13369-022-07044-5

[34] J.J. John Jeya Kamaraj, P. Annamalai, L.D. Stephen Tamil, S.P. Muthu, R. Perumalsamy, H. Valdes, Enhanced Photocatalytic Degradation of $ZnTiO_3$/Polycarbazole (PCz) Composite Towards Toxic Azo Dye, Arab. J. Sci. Eng. 48 (2023) 8143–8151. https://doi.org/10.1007/s13369-022-07570-2

[35] W. Raza, M.M. Haque, M. Muneer, M. Fleisch, A. Hakki, D. Bahnemann, Photocatalytic degradation of different chromophoric dyes in aqueous phase using la and Mo doped TiO_2 hybrid carbon spheres, J. Alloys Compd. 632 (2015) 837–844. https://doi.org/10.1016/j.jallcom.2015.01.222

[36] E.M. Bayan, T.G. Lupeiko, L.E. Pustovaya, M.G. Volkova, Synthesis and photocatalytic properties of Sn-TiO_2 nanomaterials, J. Adv. Dielectr. 10 (2020) 1–10. https://doi.org/10.1142/S2010135X20600188

[37] P. Nyamukamba, L. Tichagwa, S. Mamphweli, L. Petrik, Silver/Carbon Codoped Titanium Dioxide Photocatalyst for Improved Dye Degradation under Visible Light, Int. J. Photoenergy 2017 (2017). https://doi.org/10.1155/2017/3079276

[38] X.Q. Cheng, C.Y. Ma, X.Y. Yi, F. Yuan, Y. Xie, J.M. Hu, B.C. Hu, Q.Y. Zhang, Structural, morphological, optical and photocatalytic properties of Gd-doped TiO_2 films, Thin Solid Films 615 (2016) 13–18. https://doi.org/10.1016/j.tsf.2016.06.049

[39] R. Ebrahimi, A. Maleki, R. Rezaee, H. Daraei, M. Safari, G. McKay, S.M. Lee, A. Jafari, Synthesis and Application of Fe-Doped TiO_2 Nanoparticles for Photodegradation of 2,4-D from Aqueous Solution, Arab. J. Sci. Eng. 46 (2021) 6409–6422. https://doi.org/10.1007/s13369-020-05071-8

[40] A. Sikirman, J. Krishnan, Photocatalytic Degradation of Methylene Blue by Nanosized Visible Light Active Nitrogen and Iron co-doped Titania: Characterization and Feasibility Investigation, J. Environ. Eng. 142 (2016) 1–8. https://doi.org/10.1061/(asce)ee.1943-7870.0001028

[41] N.N. Ilkhechi, N. Ghobadi, M.R. Akbarpour, Enhanced optical and photo catalytic properties of V and La co-doped TiO_2 nanoparticles, J. Mater. Sci. Mater. Electron. 28 (2017) 6426–6434. https://doi.org/10.1007/s10854-016-6328-x